IEICE TRANS. ELECTRON., VOL.E99–C, NO.3 MARCH 2016

INVITED PAPER *Special Section on Progress towards System Nanotechnology*

Nanophotonic Devices Based on Semiconductor Quantum Nanostructures

Kazuhiro KOMORI[†a)], **Takeyoshi SUGAYA**[†], ***Members***, **Takeru AMANO**[†], ***Nonmember***, ***and*** **Keishiro GOSHIMA**[††], ***Member***

SUMMARY In this study, our recent research activities on nanophotonic devices with semiconductor quantum nanostructures are reviewed. We have developed a technique for nanofabricating of high-quality and high-density semiconductor quantum dots (QDs). On the basis of this core technology, we have studied next-generation nanophotonic devices fabricated using high-quality QDs, including (1) a high-performance QD laser for long-wavelength optical communications, (2) high-efficiency compound-type solar cell structures, and (3) single-QD devices for future applications related to quantum information. These devices are expected to be used in high-speed optical communication systems, high-performance renewable energy systems, and future high-security quantum computation and communication systems.

key words: *nanophotonic devices, quantum nanostructures, quantum dots, semiconductor lasers, solar cell devices, quantum information devices*

1. Introduction

Recent advances in nanotechnologies have enabled the fabrication of very fine nano-structures, such as quantum wires and quantum dots (QDs) [1], [2], whose sizes are controlled at the atomic-layer level by the bottom-up nanofabrication method, and of a single-quantum-nanostructure devices such as single/coupled-QD (SQD/CQD) devices for quantum information applications [3], [4] by both the bottom-up and top-down nanofabrication methods.

Semiconductor quantum nanostructures are expected to results in both quantitative and qualitative technological-advancements in photonic devices/systems; such nanostructures include quantum wires and QDs, where the density of the state can be controlled artificially by changing both the size of quantum structures and quantum confinement.

With respect to the quantitative technological innovation of optical devices, QDs are expected to enable both a significant reduction of the threshold current density of semiconductor lasers and temperature-insensitive laser operation. Moreover, the sub-bands engineering of the QDs is expected to results in a dramatic increase of the efficiency of solar cells.

With respect to qualitative technological innovations, the feature of the artificial atomic state of QDs enables them to be used in new applications of quantum information devices such as single- and entangled-photon sources as well as quantum-logic-gate devices.

We have developed new methods for fabricating high-quality QDs ensemble structures with high uniformity and high density. On the basis of these technologies, we have investigated a high-performance semiconductor laser for long-wavelength optical communication and a novel solar cell fabricated using high density quantum dots. We have also proposed and studied the novel quantum information devices based on the optical control of excitons in high quality SQD and CQD.

In this study, we review our research activities related to the nanophotonic devices based on semiconductor quantum nanostructures, including (1) a high-performance QD laser for long-wavelength optical communications, (2) a high-efficiency compound-type solar cell fabricated using QDs, and (3) single-quantum-nanostructure (SQD/CQD) devices for future applications related to quantum information.

2. Semiconductor Lasers with Highly Dense and Uniform QDs

2.1 Highly Dense and Uniform QDs

QDs have been utilized for their excellent performance in practical applications; they enable the fabrication of high-quantum-efficiency devices that are insensitive to temperature [5], [6]. Specifically, QD lasers and optical devices with a zero-dispersion wavelength of 1.3 μm have been fabricated on GaAs substrates as new luminescent materials. Moreover, QD lasers can operate at a high modulation speed without exhibiting temperature dependence and at a low threshold current density below 10 A/cm^2. However, QDs have a very small number of carriers in fundamental energy levels. Furthermore, we have not realized the exact function of δ because of QDs' size distribution. QD lasers have not been extensively adopted because of these performance limitations and poor optical gains. The density and uniformity of QDs are very important characteristics with respect to the realization of a high-performance QD laser. Many researchers have proposed various methods to prepare QDs with high and uniform density [7], [8]. Highly uniform self-assembled QDs with a full width at half maximum (FWHM) narrower than 15 meV have been prepared through numerous improvements in synthesis techniques, but QD density remains poor [9].

Manuscript received July 18, 2015.

[†]The authors are with National Institute of Advanced Industrial Science and Technology (AIST), Tsukuba-shi, 305–8568 Japan.

[††]The author is with Aichi Institute of Technology, Toyota-shi, 470–0392 Japan.

a) E-mail: k-komori@aist.go.jp

DOI: 10.1587/transele.E99.C.346

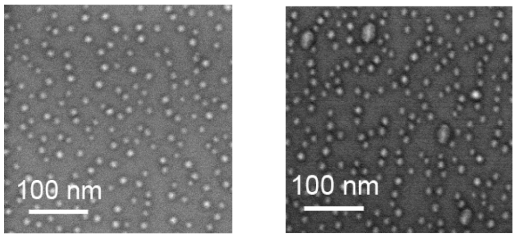

Fig. 1 Scanning electron microscope (SEM) micrographs of InAs QDs grown using (a) As_2 and (b) As_4 sources.

Numerous approaches to prepare high-density QDs have been reported, many of which involve new Sb- or N-containing materials [10]–[15]. Some QDs containing Sb exhibit densities as high as 1×10^{11} cm^{-2}; however, these materials exhibit poor crystal quality. Our main goal is to achieve high laser performance using high-density, high-uniformity, and high-quality QDs. We have proposed the fabrication of high-performance QDs using an As_2 source grown by molecular beam epitaxy (MBE). In this chapter, we report the fabrication of high-performance QDs with a density of 1×10^{11} cm^{-2} and a narrow-photoluminescence (PL) FWHM of 22.3 meV; these QDs were fabricated using As_2, a graded strain-reducing layer, and a molecular beam with a wavelength of 1.3 μm. In addition, we report the fabrication of a laser diode using these high-density and high-uniformity QDs; the resulting laser diode exhibits an optical gain greater than 8 cm^{-1} per QD layer. Moreover, we clarify optical properties of these high-density and high-uniformity QDs. Furthermore, we propose a new half-etching-mesa (HEM) laser structure, which exhibits a low threshold current of 7 mA in a short cavity length of 0.75 mm.

2.2 Optical Properties of High-Density and High-Uniformity QDs

Self-organized InAs/GaAs QD structures were grown with a high density on a GaAs(001) substrate using MBE with an As_2 source generated by a valved cracker cell [9], [16]. Coauthor Sugaya has reported that As_2 and As_4 sources have different migration lengths in cases of quantum wires and QDs. Characteristics of high-density QDs fabricated using an As_2 source differ from those of high-density QDs fabricated using an As_4 source because of the difference in the surface migration behavior of Indium atoms on surface structures generated using As_2 and As_4 sources. Figures 1 (a) and 1 (b) show scanning electron microscope (SEM) micrographs of InAs QDs grown using As_4 and As_2 sources, respectively. The InAs supply and growth temperature were 2.4 monolayers (MLs) and 570°C, respectively. Under these conditions, we achieved the same QD density of 8.0×10^{10} cm^{-2} per QD layer using As_4 and As_2 sources, as evident in the SEM micrographs. In addition, coalescent dots are evident only in Fig. 1 (a), where the dots were grown using the As_4 source. Thus, using the As_2 source, we fabricated high-density QDs without the formation of coalescent dots.

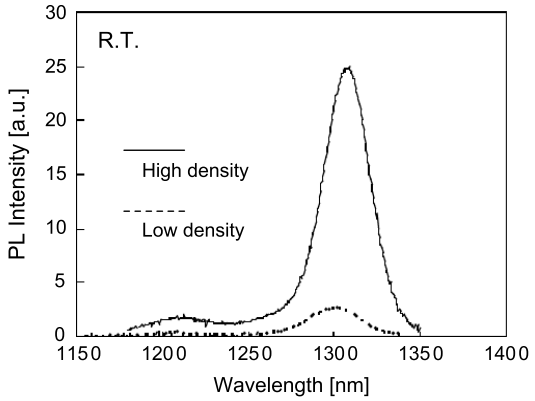

Fig. 2 Room-temperature photoluminescence (PL) spectra of high- and low-density quantum dots (QDs).

Each sample was grown under an As_2 flux of 5×10^{-6} Torr. After a GaAs buffer layer was grown at 590°C, QD structures with an InGaAs graded-composition strained relaxation layer (GC-SRL) were grown. The InAs supply and growth temperature of QDs were 2.4 ML and 540°C, respectively. The gradient composition of the GC-SRL could be controlled by changing the Ga flux. In this sample, initial and final compositions of indium in the GC-SRL layer were 23% and 10%, respectively. After the GC-SRL was grown, a 200-nm-thick GaAs barrier layer was grown. Another QD layer was grown on the surface of the GaAs barrier layer for SEM observations; this second QD layer was grown under conditions similar to those used for the inner QD layer. PL measurements and SEM observations were performed to characterize optical properties, dot size, and surface density of QDs. Figure 2 shows experimental results of room-temperature PL measurements of both our high-density (8.0×10^{10} cm^{-2}) and low-density (8.0×10^{9} cm^{-2}) QD materials. In both cases, the PL peak intensity of the ground state at 1.3 μm was saturated. Moreover, both samples exhibited a long wavelength of maximum PL intensity and a narrow FWHM of 1310 nm and 25 meV, respectively. The enhancement of the PL intensity of the ground state of high-density QDs was ten times greater than that of the ground state of low-density QDs because of an increase in QD number. Our high-density QDs exhibited a large enhancement of their PL intensity because of their high quality. We believe that our method of fabricating high-density and high-uniformity QDs using a GC-SRL and an As_2 source represents a novel technique. Thus, high-performance optical devices can be fabricated using our QDs.

We also performed lifetime measurements of these QDs. QDs with a short lifetime are necessary for the fabrication of QD lasers with high-speed modulation. Figure 3 shows the results of photon lifetime measurements at 14 K for the ground energy level of high- and low-density QDs. These measurements were performed using a high-power laser with an emission wavelength of 800 nm in conjunction with a cooled charge-coupled-device (CCD) detector. The

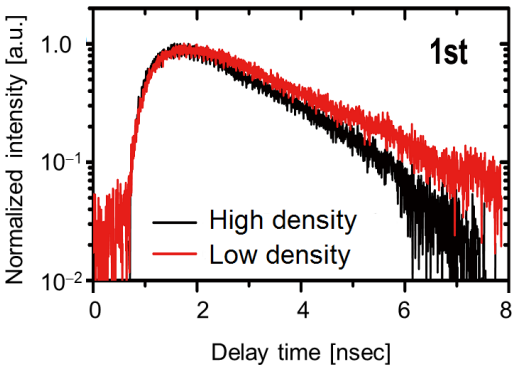

Fig. 3 Photon lifetime characteristics of high- and low-density QDs.

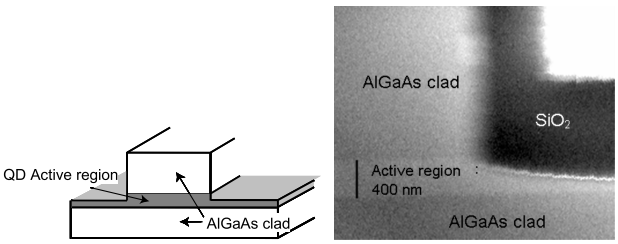

Fig. 4 (a) Schematic of a quantum-dot (QD) laser with a half-etching-mesa (HEM) structure; (b) SEM image of the HEM structure fabricated by inductively coupled plasma dry etching.

relaxation rate of high-density QDs was higher than that of low-density QDs. Radiactive lifetimes estimated from the relaxation rates for high- and low-density QDs were 1.6 ns and 2.0 ns, respectively. High-density QDs exhibit a short lifetime because of numerous emissions in their active region. On the basis of these results, we expect high-density QDs to exhibit enhanced and accelerated emissions in laser applications.

2.3 QD Lasers with a Half-Etching-Mesa Structure

InAs QD laser wafers were grown by MBE on Si-doped (100) GaAs substrates using a valved cracker cell, which was used to generate As_2. The active region consisted of nine layers of 2.4 MLs of InAs QDs with a high QD density of 6.8×10^{10} cm^{-2}, an $In_{0.25}Ga_{0.75}As$ GC-SRL with a thickness of 2.5 nm, and a GaAs barrier layer with a thickness of 38 nm [7], [17]. A new proposed QD stripe laser with an HEM structure was proposed, as shown in Fig. 4 (a). The HEM fabricated by dry etching was stopped at the center of the active region. An SEM micrograph of the fabricated HEM structure is shown in Fig. 4 (b).

The etching depth at the center of the active region was controlled by performing Cl_2/Ar inductively coupled plasma etching at a slow rate. The measurements show the structure of a laser interference microscope. An etching stop layer and clad layer were etched in the middle and stopped at the active layer structure. The etching was stopped in the middle of the active layer, where the refractive index of light

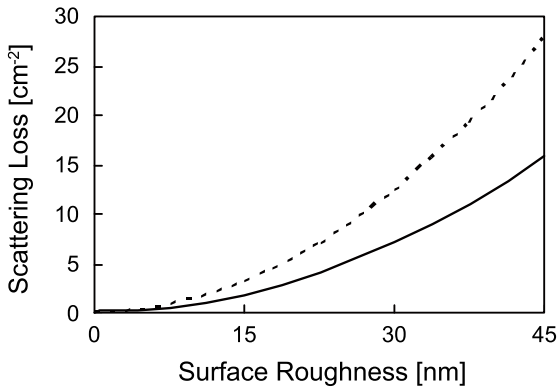

Fig. 5 Scattering loss vs. surface roughness in the HEM structure and the high-mesa waveguide.

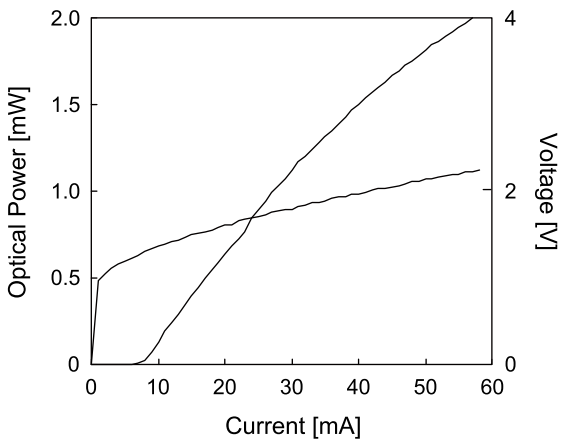

Fig. 6 Light output power of a QD HEM laser with the high mirror loss of 16 cm^{-1}.

was disturbed by the interference of QDs. As such, the etch depth was readily measured using a laser interference microscope. The HEM structural feature is intermediate between the active layer and depth of etch mesa to reduce scattering losses. We calculated the scattering losses of the HEM and high-mesa waveguide as a function of surface roughness, as shown in Fig. 5.

If the mesa width is assumed to be 1.3 μm, then 1.5 μm wavelength transmission is also assumed. The scattering loss of the HEM waveguide was reduced to almost half that of the high-mesa waveguide. All QD lasers had uncoated facets and were tested at room temperature under pulsed conditions using 2.0 μs pulses with a duty cycle of 1%. The light output vs. current characteristics of the QD HEM laser with a 0.75 mm short cavity and cleaved facet were determined at room temperature, as shown in Fig. 6.

A low-threshold-current operation of the QD laser was achieved at 7 mA and 1.3 μm emission because of the high quality of QDs and low scattering loss of the HEM structure. The mirror loss of this QD laser with short cavity and cleaved facet was high, i.e., 16 cm^{-1}; the mirror loss of the QD laser with a low-threshold-current density was 7 cm^{-1} [7]. Figure 7 shows the threshold current density vs.

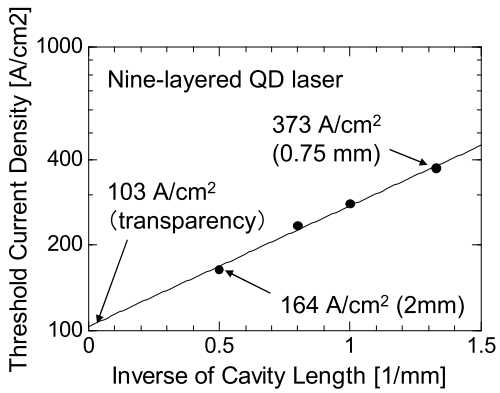

Fig. 7 The threshold current density vs. inverse cavity length in a QD laser with HEM structure

inverse cavity length for the nine-layered QD laser.

The threshold current density at which ground-state emission was observed decreased from 373 A/cm^2 in the case of the 0.75 mm short cavity to 164 A/cm^2 in the case of a 2.0 mm long cavity. Moreover, a transparency current density of 103 A/cm^2 was determined in the nine-layered QD laser with high QD density and high uniformity. We compared the threshold current density of the HEM laser with the lowest current density of the QD laser for both high- and low-density QDs. The lowest-threshold-current density for each QD layer was 7 A/cm^2/layer at a QD density of 1.4×10^{10} cm^{-2} [6]. The threshold current density for each QD layer of our proposed QD laser was 18.2 A/cm^2/layer. Moreover, the threshold current density for each QD in our proposed QD laser exhibited a lower value of 2.7×10^{-10} [A/QD number] than one of 5 x 10^{-10} [A/QD number] in QD laser with the lowest threshold current density because of the high quality of QDs and the low scattering loss of the HEM structure.

In this study, we fabricated high-performance QDs with a high density of 1×10^{11} cm^{-2} and a narrow PL FWHM of 22.3 meV using As_2, a graded strain-reducing layer, and a molecular beam at 1.3 μm. We determined optical properties of the active layer composed of high-density and high-uniformity QDs. Relaxation was also determined, and early emission with a tenfold intensity enhancement compared with that of the low-density samples was observed. High-density and high-uniformity QDs have also been demonstrated to exhibit superior optical properties. We have proposed and fabricated a 1.3 μm QD laser with an HEM stripe structure. We achieved a low-threshold-current operation of the QD laser at 7 mA with a high mirror loss of 16 cm^{-1} at 1.3 μm emission because of the high quality of QDs and the low scattering loss of the HEM structure. Furthermore, we achieved a low-threshold-current density of 2.7×10^{-10} [A/QD number], which is lower than that of the QD laser with the lowest reported threshold current density. We believe that our proposed high-density 1.3-μm QD fabrication method using a GC-SRL, an As_2 source, and an HEM waveguide structure represents a breakthrough fabrication technique for QD lasers.

3. Ultra-High-Stacked QD Structures and Their Application to Solar Cell Devices

3.1 QD Structures for Solar Cell Devices

Increasing demand for renewable energy indicates that we can expect photovoltaic technologies to become less expensive and to provide exceptionally high conversion efficiencies. QD solar cells (intermediate-band solar cells) have recently been investigated extensively and are expected to provide a conversion efficiency greater than 60% under concentrator conditions [18]. QD superlattice structures are inserted into a p–n junction of matrix materials for intermediate-band solar cells. The realization of such high-efficiency solar cells necessitates the fabrication of highly stacked QD superlattice structures that are uniform and distributed periodically in all three dimensions [19]. Although the InAs/GaAs QD material system has been studied, most of these QDs have been grown by solid-source MBE, where the crystal quality of InAs/GaAs QDs degrades as the number of QD layers increases because of the buildup of internal strain. Therefore, the InAs/GaAs QD solar cell performance also degrades as the number of QD layers increases [20]. To overcome these problems, a strain balancing growth technique involving the deposition of GaNAs buffer layers has been demonstrated for InAs/GaAs material systems [21]. InGaAs QDs are alternative candidates for stacked structures because of their small lattice mismatch with a GaAs substrate. In this study, we review the fabrication of high-quality and ultra-high stacks of 400-layer $In_{0.4}Ga_{0.6}As$ QD structures without using a strain balancing growth technique. 150-stack $In_{0.4}Ga_{0.6}As$ QD solar cells exhibit good cell performance, which, to the best of our knowledge, has not been reported for any other material systems. Moreover, we report the fabrication of InGaP-based InGaAs QD solar cells as optimal intermediate-band solar cells.

3.2 Fabrication of Ultra-High-Stacked QD Structures

We grew 20- to 400-stack $In_{0.4}Ga_{0.6}As$ QD layers on Si-doped GaAs (001) substrates using an As_2 source without using a strain balancing technique. As_2-grown multistacked InGaAs QD structures exhibit superior optical properties compared with those of As_4-grown structures grown at a high growth rate of 1 μm/h [22], [23]. The thicknesses of the $In_{0.4}Ga_{0.6}As$ QD and GaAs barrier layers were 2 nm and 20 nm, respectively. The growth temperature was 520°C. Figure 8 shows a cross-sectional scanning transmission electron microscopy (STEM) image of the top portion of 300-stack $In_{0.4}Ga_{0.6}As$ QD layers. $In_{0.4}Ga_{0.6}As$ QDs exhibit a diameter of approximately 30 nm and a height of approximately 7 nm; they are aligned 55° – 65° relative to the (001) surface. No dislocations were generated after 300 layers were stacked, although no strain balancing was employed during the growth.

Figure 9 shows PL spectra of 20- to 400-stack

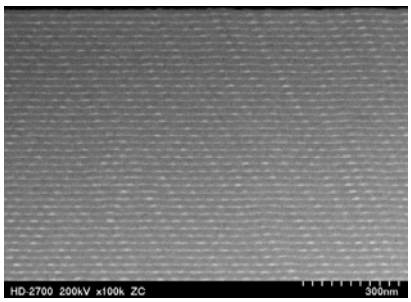

Fig. 8 Cross-sectional scanning transmission electron microscopy (STEM) images of the top portion of 300-stack $In_{0.4}Ga_{0.6}As$ QD layers. No dislocations were generated after 300 layers were stacked, although no strain balancing was employed during the growth.

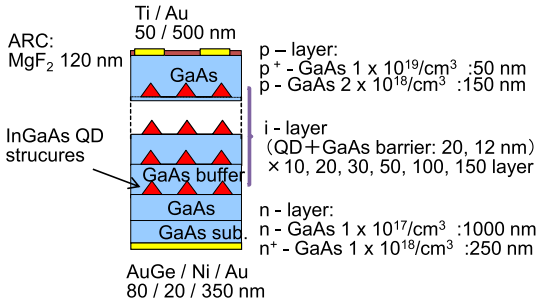

Fig. 10 Schematic layer structure of a multistacked InGaAs/GaAs QD solar cell grown on a GaAs (001) substrate.

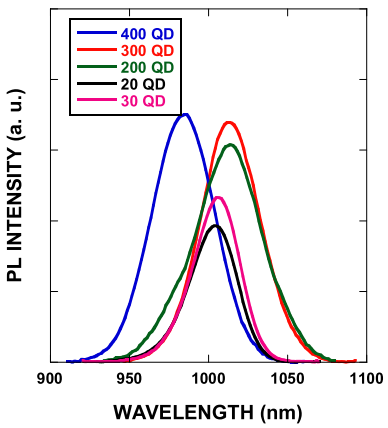

Fig. 9 PL spectra of 20-, 30-, 200-, 300-, and 400-stack $In_{0.4}Ga_{0.6}As$ QD layers at 11 K.

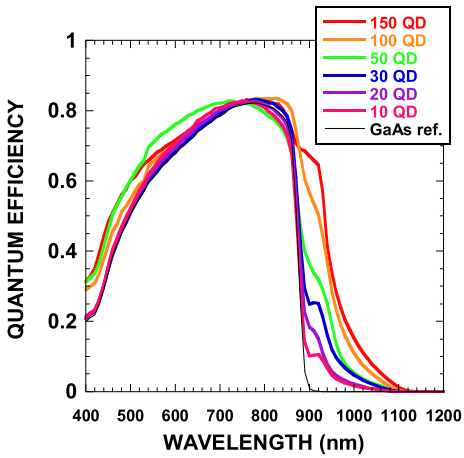

Fig. 11 EQE spectra of multistacked $In_{0.4}Ga_{0.6}As$ QD solar cells and a GaAs reference cell.

$In_{0.4}Ga_{0.6}As$ QD layers at 11 K. PL intensities of 200-, 300-, and 400-stack QDs are higher than those of 20- and 30-stack QDs with high-quality crystals [23]. Because all 400-layer QDs are not excited by an Ar^+ laser (λ = 514.5 nm), PL originates mainly from the upper portions of stacked structures and reflects the quality of crystals in those regions. The abovementioned results indicate the growth of high-quality and ultra-high stacks of $In_{0.4}Ga_{0.6}As$ QD structures even after 400 layers without using any special strain balancing method. 300- and 400-stack $In_{0.4}Ga_{0.6}As$/GaAs QD structures are believed to be still in the critical thickness. The difference in the PL wavelength is attributed to different QD sizes resulting from different growth interruption times [24].

3.3 Application to Solar Cell Devices

The sample structure of solar cell devices is described in Fig. 10, where i-layer multistacked QD structures were inserted into the GaAs p–n junction [24]. The i-layer region consists of 10-, 20-, 30-, 50-, 100-, and 150-stack 2-nm $In_{0.4}Ga_{0.6}As$ QD structures. The barrier-layer thicknesses between QDs were 12 nm and 20 nm for 150-stack and other structures, respectively.

Figure 11 shows EQE spectra of multistacked $In_{0.4}Ga_{0.6}As$ QD solar cells and a GaAs reference cell. The EQE of the cells has extended photoabsorption spectra to wavelengths longer than the GaAs bandgap. Photoabsorption at wavelengths greater than 900 nm by multistacked $In_{0.4}Ga_{0.6}As$ QD structures increases as the number of stacking layer increases. $In_{0.4}Ga_{0.6}As$ QD solar cells show good EQE spectra even after 150 QD layers were stacked, which indicates that InGaAs QDs are suitable for use in highly stacked QD solar cells with high efficiency.

Figure 12 shows I–V curves of multistacked $In_{0.4}Ga_{0.6}As$ QD solar cells with various numbers of QD layers and the curve of a GaAs reference cell. The parameters of each solar cell are reported in Table 1. The short-circuit current density J_{sc} increased from 17.5 to 23.6 mA/cm^2 as the number of stacking layers increased. Although the open-circuit voltage (V_{oc}) decreases as the number of stacking layers increases, as shown in Fig. 5, the V_{oc} becomes almost saturated when the number of stacking layers exceeds 50. The conversion efficiency of the 50-stack QD solar cell is higher than that of the 30-stack QD cell. $In_{0.4}Ga_{0.6}As$ QD solar cells exhibit good cell characteristics even after an ultra-high stacking of 150 QD layers. Such good cell performance has not been reported for 100-stack QD solar cells fabricated using other materials.

The V_{oc} value, shunt resistance, and conversion efficiency decrease in thick-layer QD solar cells. These

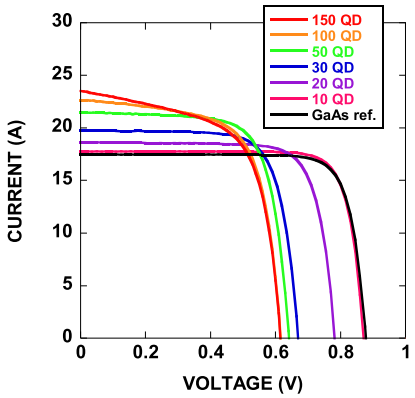

Fig. 12 *I–V* curves of multistacked $In_{0.4}Ga_{0.6}As$ QD solar cells with various QD layers and the *I–V* curve of a GaAs reference cell.

Table 1 Parameters of multistacked $In_{0.4}Ga_{0.6}As$ quantum dot (QD) solar cells with various numbers of QD layers and the parameters of a GaAs reference cell.

QD layers	10	20	30	50	100	150	GaAs. ref.
Efficiency (%)	12.4	11.3	9.8	10.0	9.4	9.2	12.4
V_{oc} (V)	0.868	0.783	0.671	0.643	0.616	0.616	0.878
J_{sc} (mA/cm^2)	17.7	18.7	19.7	21.5	22.7	23.6	17.5
FF	0.805	0.774	0.743	0.724	0.670	0.630	0.809

phenomena are believed to be due to inefficient collection and recombination of carriers in QD regions. The energy difference between the GaAs conduction band and InGaAs QD state is 0.2–0.3 eV. This value is extremely small for additional photoabsorption from the solar spectrum because the spectrum contains few low-energy photons. Therefore, we cannot utilize two-step photoabsorption. Other material systems may need to be explored to enlarge the energy difference between the conduction band and QD state.

3.4 InGaP-Based QD Solar Cells

When the bandgap of a matrix semiconductor is 1.9 eV, optimal intermediate-band solar cells with a conversion efficiency of 60% are expected [18]. InGaP with a bandgap of 1.9 eV is a suitable matrix material with which optimal intermediate-band solar cells can be realized. Although the solid-source MBE technique is suitable for growing a QD structure, as previously discussed, InGaP is very difficult to grow. InGaP solar cells are grown by metal-organic chemical vapor deposition, and the literature contains few reports on InGaP solar cells fabricated using solid-source MBE. In this study we use InGaP as a matrix semiconductor for QD solar cells grown by solid-source MBE [25], [26].

We grew 10- and 20-stack $In_{0.4}Ga_{0.6}As$ QD layers with 2-nm-thick GaAs spacer layers without using a strain balancing growth technique. We controlled the energy difference between the $In_{0.48}Ga_{0.52}P$ conduction band and

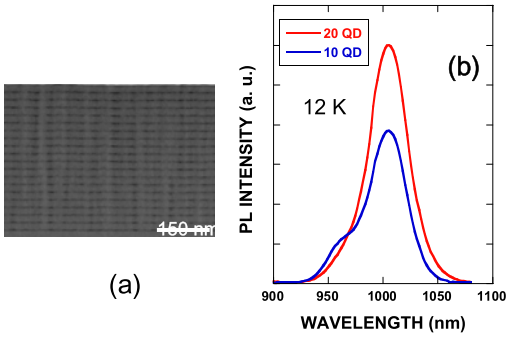

Fig. 13 (a) A STEM image and (b) PL spectra of multistacked InGaAs QD layers with 2 nm GaAs spacer layers and 16-nm-thick InGaP barriers.

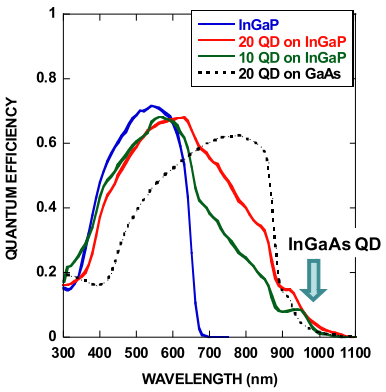

Fig. 14 EQE spectra of InGaP-based multistacked InGaAs QD solar cells with GaAs spacer layers with a reference InGaP solar cell. The dotted line indicates the EQE spectrum of the GaAs-based InGaAs QD solar cell.

QD energy state using GaAs spacer layers [26]. The thickness of InGaP barrier layers between the $In_{0.4}Ga_{0.6}As$ QDs and GaAs spacer was 16 nm, which indicates a thickness of 20 nm between QD layers. We used a 7 s interruption between the growth of InGaP and GaAs to switch the group-V flux. The growth temperature was 480°C for both InGaP layers and InGaAs QD structures.

Figure 13 (a) shows STEM images of 20-stack InGaAs QD layers with 2-nm GaAs spacer layers and 16-nm-thick InGaP barrier layers. InGaAs QDs with a diameter of 20–30 nm and a height of 7 nm are observed to be well aligned in the growth direction. Figure 13 (b) shows PL spectra of 10- and 20-stack InGaAs QD layers measured at 12 K. PL spectral peaks of multistacked QDs become more intense and narrower as the number of stacking layers increases: these spectral features indicate that high-quality multistacked InGaAs QD structures with GaAs spacer layers in an InGaP matrix were grown without using any special strain balancing method.

Figure 14 shows EQE spectra of InGaP-based multistacked InGaAs QD solar cells with 20 nm GaAs spacer layers. EQEs of 10- and 20-stack QD solar cells and that of an InGaP reference cell are shown. The dotted line indicates the EQE spectrum of a GaAs-based 20-stack InGaAs

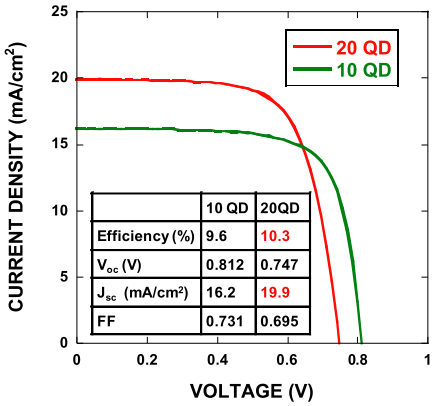

Fig. 15 I–V curves of InGaP-based multistacked InGaAs solar cells with GaAs spacer layers.

QD solar cell as a reference. The photoabsorption of InGaP-based QD structures at wavelength greater than 650 nm increased as the number of stacking layers increased, where the absorption from 650 to 870 nm is due to the GaAs spacer layers. The peaks at 920–950 nm are believed to be due to the photoabsorption of InGaAs wetting layers. The photoabsorption of InGaAs QDs is observed at approximately 1000 nm. Although the photoabsorption of the QDs is small, InGaP-based InGaAs QDs exhibit grater photoabsorption than GaAs-based QD structures.

Figure 15 shows *I*–*V* curves of InGaP-based 10- and 20-stack InGaAs QD solar cells with a 120 nm MgF_2 anti-reflection coating. The J_{sc} increased from 16.2 to 19.9 mA/cm^2 as the number of stacking layers increased. As shown in Fig. 12, the J_{sc} of 19.9 mA/cm^2 is larger than that of the GaAs-based 20-stack InGaAs QD solar cell (18.7 mA/cm^2). This greater J_{sc} is attributed to the InGaP-based InGaAs QD system exhibiting photoabsorption over a wider wavelength region. Moreover, the conversion efficiency increases as the number of QD layers increases in the InGaP-based system, although the efficiency of GaAs-based QD solar cells decreases with an increasing number of QD layers.

The V_{oc} value decreases with an increasing number of stacked QD layers, as shown in Fig. 8, which is the same phenomenon observed in Fig. 12. Because InGaP-based QD solar cells have no QD minibands, we cannot utilize two-step photon absorption. Therefore, QD solar cells still exhibit low V_{oc}, as shown in Fig. 15. However, V_{oc} might be improved through the use of QD minibands because of the increased carrier lifetime in an intermediate band for the two-step photon absorption. Highly stacked InGaAs QD minibands are needed in InGaP matrix layers to increase the V_{oc} and J_{sc} by utilizing two-step photon absorption.

In this chapter, we report the fabrication of ultra-high-stacked and high-quality $In_{0.4}Ga_{0.6}As$/GaAs QD solar cells without using any strain balancing technique. The intensity of EQE spectra and J_{sc} of QD solar cells increase as the number of $In_{0.4}Ga_{0.6}As$ QD layers increases to 150. We have also reported $In_{0.48}Ga_{0.52}P$-based 10- and 20-stack $In_{0.4}Ga_{0.6}As$ QD solar cells with GaAs spacer layers fabricated using solid-source MBE. The J_{sc} and conversion efficiency of InGaP-based QD solar cells increase with increasing number of QD layers. InGaP-based QD solar cells are very attractive for use in the fabrication of optimal intermediate-band solar cells.

Various authors have reported a reduction in V_{oc} due to carrier recombination in QD solar cells [20], [21], [27], which is a problem that must be overcome. The reduced V_{oc} in QD solar cells can be improved through two-step photoabsorption because carrier recombination is reduced in QD regions. Two-step photoabsorption has been reported to be induced through the optical transition from the InAs QD state to GaNAs conduction band in a Si-doped QD solar cell under infrared-light illumination conditions [28]. The authors of this previous report indicated that photocurrent can be increased by two-step photon absorption if appropriate doping and a suitable excitation source for the optical transition from the QD state to conduction band are used. If we are to utilize two-step photon absorption, a sufficiently large energy difference must exist between the QD energy state and conduction band of matrix materials because the thermally assisted carrier transition must be suppressed [29]. In addition, the carrier lifetime in QD minibands should be increased to achieve two-step photon absorption [30]. We have reported the formation of electronically coupled InGaAs QD states [31], [32] and increased photocurrent in InGaAs/GaAs QD solar cell structures [33]. Therefore, InGaP-based QD miniband solar cells are very attractive for use in realizing optimal intermediate-band solar cells to increase V_{oc} and J_{sc} via two-step photon absorption.

4. Fabrication of Quantum Information Devices Using Semiconductor-Coupled QDs

4.1 Fabrication of Quantum Logic Gates Using Excitons in Coupled QDs

QDs are considered attractive candidates for quantum information devices because their atom-like properties can be engineered via nanofabrication [34], [35]. Moreover, exciton coherence can be optically controlled and monitored using an ultrafast (femtosecond to picosecond time domain) spectroscopy technique [36], [37]. The long duration of exciton coherence in QDs, originating from the superposition of ground and excited states, has enabled the fabrication of a quantum bit (qubit), which is the fundamental unit of quantum computation [3], [38]. The realization of two fundamental quantum logic gates of a rotation gate (one-qubit) and a controlled rotation gate (two-qubit) using exciton states in QDs is required for the successful implementation of quantum computation [4].

In the case of one-qubit gates, exciton Rabi oscillation in InGaAs/GaAs QDs [39] and InGaAs/AlGaAs QDs [40] has been reported. With respect to two-qubit gates, optically driven QDs have been proposed as a quantum

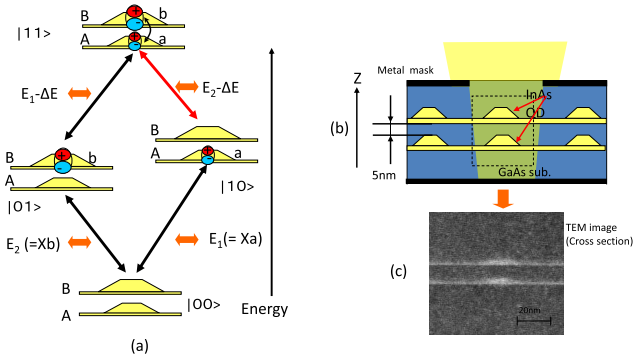

Fig. 16 Diagram of a two-qubit exciton system using a coupled QD (CQD): (a) Four-level exciton diagram with a CQD system, where α, β (= 0 or 1) of $|\alpha,\beta>$ shows the exciton states of QD A and QD B, respectively; |00>, |01>, |10>, and |11> denote the crystal ground state, and ΔE indicates the binding energy of the correlated-exciton molecule. (b, c) Schematic and STEM image of InAs/GaAs CQDs.

information system [41]. Chen et al. have proposed a four-level system comprising excitons and biexcitons in SQDs [42], [43]. However, increasing the number of qubits is difficult. Consequently, we proposed a two-qubit quantum logic gate using artificial exciton molecule states; this logic gate consists of two different excitons confined in each QD of a CQD [44]–[46] for multiqubit applications. The application of this device to quantum information processing requires the three technical steps as follows: (1) the creation of a four-level system using four-exciton states (a crystal ground state |00>, on exciton states of |01> and |10>, and an artificial exciton molecule state of |11>) in a CQD; (2) arbitrary control of the probability density—specifically, populations and coherences—of four-exciton states via cascade optical excitation; and (3) the demonstration of a two-qubit-controlled rotation (CROT) gate. In this section, we describe our recent studies on quantum information devices based on exciton molecule states in a CQD.

Figure 16 (a) shows the transition energy diagram and two-qubit exciton states of CQDs, where |00>, |01>, and |10>, |11> are the crystal ground state, one-exciton state, and two-exciton states of the CQDs, respectively. In this four-level, two-qubit exciton system of |00>, |10>, |01>, and |11>, the most important and difficult technology for the realization of two-qubit quantum logic gates is the formation of new states of the correlated-exciton molecule state |11> using an exciton confined in each QD of a CQD and the formation of exciton correlation ($\Delta E \neq 0$).

The transition energy between the crystal ground state (|00>) and one-exciton state (|01>) is E_2 and that between the one-exciton state (|10>) and correlated-exciton molecule state (|11>) is $E_2 - \Delta E$, where ΔE is the binding-energy shift caused by the formation of the correlated-exciton molecule. Transition energies of other excitation processes—specifically, |00> → |10> and |01> → |11> — correspond to $E1$ and $E_1 - \Delta E$, respectively. In a two-qubit exciton system, the energy shift (ΔE) of $E_1 - \Delta E$ should be the same as that of $E_2 - \Delta E$, as shown in Fig. 16 (a). The operation process of a two-qubit logic gate using these four states is shown as follows.

First, the ground state of |00> is optically excited to the state |00> + |01> by applying a $\pi/2$ pulse with a center energy (frequency) of E_1. Second, the state |00> + |01> is excited to the state |00> + |11> by applying a $\pi/2$ pulse with a center energy (frequency) of $E_2 - \Delta E$. Note that the state |00> does not evolve under the π pulse because of a detuning of ΔE. If a one-exciton state |01> or |10> is prepared and another exciton state is excited within a time Δt of exciton lifetime, then the entangled-exciton states of |11> are realized in CQD systems. An entangled four-level two-qubit exciton system cannot be factorized, and two excitons are entangled because of an energy shift of $\Delta E \neq 0$ [41].

4.2 Fabrication and Characterization of Quantum Logic Gates Using Excitons in a CQD

We have fabricated two-qubit logic gates using correlated excitons in a CQD [44]–[46]. Figure 16 (b) shows a structural model of a two-qubit exciton system using a CQD. The methods employed to fabricate the samples used in the experiments were the same as those reported in our previous study [46]. Self-organized InAs QD samples were grown by MBE using the indium-flush method, as shown in the cross-sectional STEM image in Fig. 16 (c). We selected a barrier thickness of 5 nm to satisfy the requirements that (1) a hole be localized in each QD to confine excitons and (2) an electron be delocalized and weakly coupled between QDs [44]. CQD samples were cooled to 6 K in a liquid helium cryostat and excited by a continuous-wave tunable Ti:sapphire laser. Luminescence from QDs was led into a double monochromator and detected using a cooled charge-coupled device. In addition, a Ti:sapphire laser providing 4-ps-long pulses at a repetition rate of 76 MHz was used for the pulse excitation control of an exciton state in QDs for Rabi oscillation measurements.

Figure 17 shows a micro-PL spectrum from a CQD with d = 5 nm used in this study. The PL spectrum has two groups, i.e., *Xa* and *Xb*, with an energy separation of 15–20 meV because of quantum mechanical coupling [44], where suffixes "*a*" and "*b*" indicate antibonding and bonding states, respectively. Moreover, each PL group consists of two peaks separated by 2–5 meV, where lower- and higher-energy peaks are indicated as *Xa_Xb_* and *X2a_X2b_*, respectively. The measurement of spin-selective optical excitation revealed that *X2a* and *X2b* peaks originate from excitons with a *p*-like hole excited state [45]. In contrast, *Xa* and *Xb* peaks originate from excitons with an *s*-like hole ground state because wavefunctions of a hole are not coupled with the neighboring QD as a consequence of the large effective mass of the hole, which leads to a small energy-level separation [45].

4.3 Optical Control of Two-Qubit States in a CQD System

In PL excitation measurements of a CQD system, we ob-

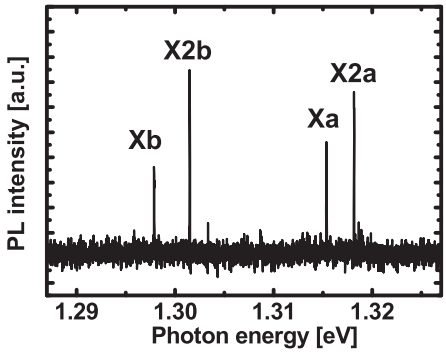

Fig. 17 PL spectra of a CQD. *Xa* and *Xb* peaks originate from antibonding- and bonding-like states in a CQD, respectively, and *X2a* and *X2b* peaks originate from antibonding- and bonding-like states with the excited state of a hole in a CQD. The PL spectrum of CQDs excited at 1.41 eV (absorption band of wetting layer), where the excitation intensity was set sufficiently low such that multiple excitons could not be excited.

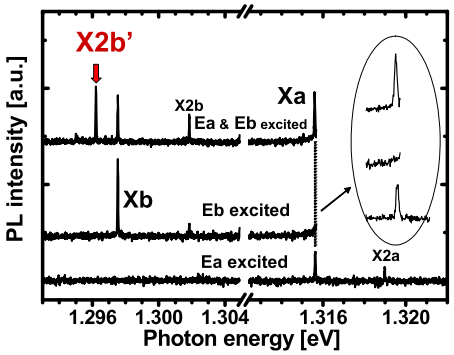

Fig. 18 PL spectra of a CQD using one-color and two-color excitations. The inherent excitation at the *Ea* (*Eb*) energy yielded only an |10> state (|01> state) emission.

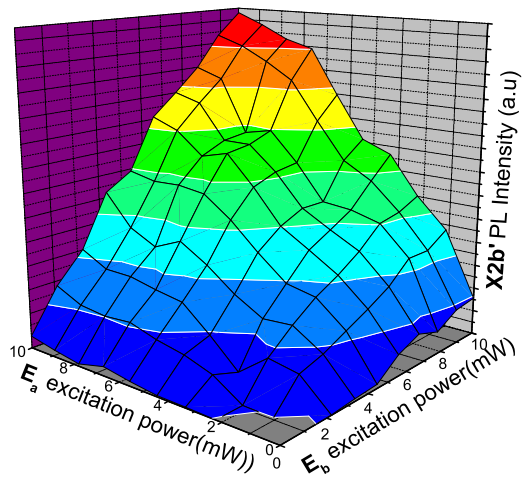

Fig. 19 The two-color excitation power dependence of the PL intensity *X2b′*, where *X* and *Y* axes show the excitation power at energies E_a and E_b, respectively.

served inherent excited states of *Ea* = 1.3231 eV and *Eb* = 1.3392 eV for |01> and |10> states, respectively [43], [45]. Thus, the creation of excitons of |01> and |10> states can be controlled individually using two laser sources. For example, when we pump at the inherent excited state of *Ea* (*Eb*), the |10> (|01>) state can be created, but the |01> (|10>) state cannot be created. Figure 18 shows PL spectra under individual (one-color) excitation or simultaneous (two-color) excitation conditions using energy-selective excitation, as previously mentioned. Excitation at the *Ea* (*Eb*) energy yielded only a |10> (|01>) emission, as shown in the center (bottom) of Fig. 18.

When |10> and |01> states were excited simultaneously using two-color excitation (both *Ea* and *Eb*), a new peak appeared on the lower-energy side of the *Xb* peak in the spectrum (labeled *X2b′* at the top of the figure). This observation directly indicates the existence of an exciton molecule in a CQD system.

To clarify the origin of the *X2b′* peak, we investigated the two-color excitation-power dependence on the intensity of the *X2b′* PL peak, as shown in Fig. 19, where the two-color excitation energies were fixed at *Ea* and *Eb* as inherent excited states. If the *X2b′* peak originates from the biexciton state |02> of *Xb* itself, the PL intensity of *X2b′* should strongly depend only on *Eb* excitation, whereas if *X2b′* originates from the correlated-exciton molecule state |11>, the PL intensity of *X2b′* should depend on both *Ea* and *Eb* excitations. The results show that the *X2b′* PL intensity depends on both *Ea* and *Eb* excitations, which indicates that the *X2b′* peak originates from the correlated-exciton molecule state of |11> created by two individual excitons.

4.4 Control of the Population of Four-Exciton States

In this section, we report exciton Rabi oscillations in SQD and CQD to control the population of four-exciton states. In addition, we show the differences between optical properties of an SQD and a single pair of CQDs to observe the exciton transition dipole moment.

Figure 20 shows the PL intensity vs. average power of the laser pulse for an SQD and a single pair of CQDs. The excitation laser energy is tuned at the excited state (E_1) of the *Xa* peak, where E_1 originates from the second excited states of holes because the first excited states of holes originate from the *X2a* peak. We observed that the PL intensity oscillates with an increase in the square root of the pump power, i.e., the pulse area. The PL intensity vs. square root of the average power can be fitted to a sinusoidal solid curve. We considered that top and bottom points correspond to the π-pulse area (θ = π) and 2π-pulse area (θ = 2π), respectively. On the basis of these experimental results, we have successfully observed Rabi oscillation between |00> and |10> states in a single pair of CQDs by controlling the input pulse area. The transition dipole moment calculated from Rabi oscillation between |00> and |10> states was 72 D, which is larger than that of an SQD in our previous studies (40 D) [47], where the transition dipole moment was derived from the value of excitation power on the surface of a sample. Thus, we experimentally observed the pulse-area control of Rabi oscillation in a single pair of CQDs. The re-

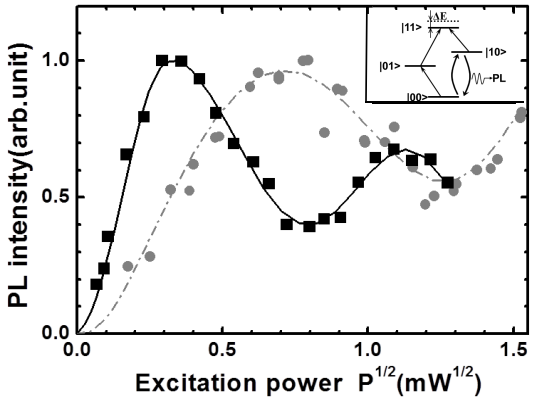

Fig. 20 The PL intensity from the ground state was recorded while the average total input laser intensity was varied for pulse area at the sample surface. Solid and dotted lines show fits to the data. Transition dipole moments of CQD and SQD are 72 and 40 D, respectively. Both PL intensities are normalized. Inset: QD energy diagram. The CQD is resonantly excited to the excited state of |10>. The population that relaxes to the ground state |00> is detected.

sults demonstrate the possibility of realizing a quantum gate with two qubits.

In this chapter, a two-qubit quantum logic gate using artificial exciton molecule states, where the logic gate consists of two different excitons confined in each QD of a CQD for multiqubit applications, was proposed. In the first part of this chapter, we demonstrated the formation and control of two-qubit exciton states consisting of a two-qubit exciton system in CQDs. In the second part of this chapter, we demonstrated an arbitrary control of the probability density—specifically, the populations and coherences—of four-exciton states via the optical control of Rabi oscillations. The results demonstrate that our device structure can be utilized as a two-qubit quantum logic gate and that a two-qubit solid-state device structure enables both ultrafast optical control and multibits.

As further work, demonstrating Rabi oscillation between |01> and |11> states will be important. In a CROT gate, the target bit (first bit) is rotated through a π-pulse area if and only if the control bit (second bit) is 1. More specifically, a π pulse tuned to the $|01> \rightarrow |11>$ transition is selected as the operational pulse for the CROT gate. When the input is only |01>, the operational pulse will rotate the input to |11>. Similarly, if an input of |11> is selected, the operational pulse will stimulate it down to |01>.

5. Conclusion

We have reviewed our recent studies on nanophotonic devices based on semiconductor quantum nanostructures. We have developed the core technologies for the fabrication of high-quality and high-density of QD structures using As_2 sources in MBE growth. On the basis of this technology, quantitative improvements of semiconductor optical devices are demonstrated. High performance 1.3um laser devices with high gain and very low threshold current density were realized using the GC-SRL technique. In addition, ultra-high-stacked QD solar cell devices were realized without the use of a strain balancing technique. Solar cell device structures with 150 layer stacked InGaAs/GaAs QD structure and a 20-layer stacked InGaAs/InGaP QD structure were realized. For application to the quantum information devices, we have proposed a two-qubit quantum logic gate using an artificial exciton-molecule state of excitons in a CQDs. We have successfully demonstrated the preliminary operation of these devices such as the formation of two-qubit states and arbitrary controls of the probability density of exciton states - specially, one-qubit operation - via the optical control of Rabi-oscillation. We expect that these new nanophotonic devices will bring about the quantitative and qualitative technological changes for the future photonic devices and systems.

Acknowledgments

These works were partially supported by **CREST**, the Japan Science and Technology Agency, and the Strategic Information and Communications R&D Promotion Program from the Ministry of Internal Affairs and Communications, and the New Energy and Industrial Technology Development Organization (NEDO) under the Ministry of Economy, Trade and Industry (METI).

References

[1] Y. Arakawa and H. Sakaki, "Multidimensional quantum well laser and temperature dependence of its threshold current," Appl. Phys. Lett., vol.40, no.11, pp.939–941, June 1982.
[2] M. Asada, Y. Miyamoto, and Y. Suematsu, "Gain and the threshold of three-dimensional quantum-box lasers," IEEE J. Quantum Electron., vol.QE-22, no.9, pp.1915–1921, 1986.
[3] A. Barenco, D. Deutsch, and A. Eckert, "Conditional quantum dynamics and logic gates," Phys. Rev. Lett., vol.74, pp.4083–4086, 1998.
[4] E. Biolatti, R.C. Iotti, P. Zanardi, and F. Rossi, "Quantum information processing with semiconductor macroatoms," Phys. Rev. Lett., vol.85, no.26, pp.5647–5650, 2000.
[5] O.B. Shchekin and D.G. Deppe, "1.3-μm InAs quantum dot laser with T_0 = 161 K from 0 to 80°C," Appl. Phys. Lett., vol.80, no.18, p.3277, 2002.
[6] H. Shimizu, S. Saravanan, J. Yoshida, S. Ibe, and N. Yokouchi, "InAs quantum dot lasers with extremely low threshold current density (7 A/cm^2/Layer)," Jpn. J. Appl. Phys., vol.44, pp.L1103–L1104, 2005.
[7] T. Amano, T. Sugaya, and K. Komori, "Highest density 1.3-μm InAs quantum dots covered with gradient composition InGaAs strain reduced layer grown with an As_2 source using molecular beam epitaxy," Jpn. J. Appl. Phys., vol.44, no.12, pp.L432–L434, 2005.
[8] T. Amano, T. Sugaya, and K. Komori, "Characteristics of 1.3 μm quantum-dot lasers with high-density and high-uniformity quantum dots," Appl. Phys. Lett., vol.89, no.17, p.171122, 2006.
[9] T. Amano, T. Sugaya, S. Yamauchi, and K. Komori, "Realization of 1.3-μm InAs quantum dots with high-density, uniformity, and quality," J. Cryst. Growth, vol.295, no.2, pp.162–165, 2006.
[10] T. Akiyama, O. Wada, H. Kuwatsuka, T. Simoyama, Y. Nakata, K. Mukai, M. Sugawara, and H. Ishikawa, "Nonlinear processes responsible for nondegenerate four-wave mixing in quantum-dot optical amplifiers," Appl. Phys. Lett., vol.77, no.12, p.1753, 2000.

[11] K. Yamaguchi, K. Yujobo, and T. Kaizu, "Stranski-krastanov growth of InAs quantum dots with narrow size distribution," Jpn. J. Appl. Phys., vol.39, no.12A, pp.L1245–L1248, 2000.
[12] K. Nishi, H. Saito, S. Sugou, and J.-S. Lee, "A narrow photoluminescence linewidth of 21 meV at 1.35 μm from strain-reduced InAs quantum dots covered by In Ga As grown on GaAs substrates," Appl. Phys. Lett., vol.74, no.8, p.1111, 1999.
[13] T. Matsuura, T. Miyamoto, T. Kageyama, M. Ohta, Y. Matsui, T. Furuhata, and F. Koyama, "Surfactant effect of Sb on GaInAs quantum dots grown by molecular beam epitaxy," Jpn. J. Appl. Phys., vol.43, no.5A, pp.L605–L607, 2004.
[14] K. Yamaguchi and T. Kanto, "Self-formation of high-uniformity and high-density quantum dots," J. Cryst. Growth, vol.275, Issues 1-2, pp.e2269–e2273, 2005.
[15] N. Yamamoto, K. Akahane, and N. Ohtani, "Growth of high-density InGaSb quantum dots on silicon atoms irradiated GaAs substrates," Physica E, vol.21, no.2-4, pp.322–325, 2004.
[16] T. Sugaya, K. Komori, S. Yamauchi, and T. Amano, "1.3 μm InAs quantum dots grown with an As-2 source using molecular-beam epitaxy," J. Vac. Sci. Technol. B, vol.23, no.3, pp.1243–1246, 2005.
[17] T. Amano, T. Sugaya, and K. Komori, "1.3-μm InAs quantum-dot laser with high dot density and high uniformity," IEEE Photon. Technol. Lett., vol.18, no.4, pp.619–621, 2006.
[18] A. Luque and A. Martí, "Increasing the efficiency of ideal solar cells by photon induced transitions at intermediate levels," Phys. Rev. Lett., vol.78, no.26, pp.5014–5017, June 1997.
[19] A. Luque, A. Martí, N. López, E. Antolín, E. Cánovas, C. Stanley, C. Farmer, and P. Díaz, "Operation of the intermediate band solar cell under nonideal space charge region conditions and half filling of the intermediate band," J. Appl. Phys., vol.99, no.9, pp.094503-1–094503-9, May 2006.
[20] A. Martí, N. López, E. Antolín, E. Cánovas, A. Luque, C.R. Stanley, C.D. Farmer, and P. Díaz, "Emitter degradation in quantum dot intermediate band solar cells," Appl. Phys. Lett., vol.90, no.23, pp.233510-1–233510-3, June 2007.
[21] Y. Okada, R. Oshima, and A. Takata, "Characteristics of InAs/GaNAs strain-compensated quantum dot solar cell," J. Appl. Phys., vol.106, no.2, pp.024306-1–024306-3, July 2009.
[22] T. Sugaya, T. Amano, M. Mori, S. Niki, and M. Kondo, "Highly stacked and high quality quantum dots fabricated by intermittent deposition of InGaAs," Jpn. J. Appl. Phys., vol.49, no.3, 030211-1–030211-3, March 2010.
[23] T. Sugaya, T. Amano, M. Mori, and S. Niki, "Highly stacked InGaAs quantum dot structures grown with two species of As," J. Vac. Sci. Technol. B, vol.28, no.3, pp.C3C4–C3C8, March 2010.
[24] T. Sugaya, O. Numakami, R. Oshima, S. Furue, H. Komaki, T. Amano, K. Matsubara, Y. Okano, and S. Niki, "Ultra-high stacks of InGaAs/GaAs quantum dots for high efficiency solar cells," Energy Environ. Sci., vol.5, no.3, pp.6233–6237, March 2012.
[25] T. Sugaya, R. Oshima, K. Matsubara, and S. Niki, "In(Ga)As quantum dots on InGaP layers grown by solid-source molecular beam epitaxy," J. Cryst. Growth, vol.378, pp.430–434, July 2013.
[26] T. Sugaya, A. Takeda, R. Oshima, K. Matsubara, S. Niki, and Y. Okano, "InGaP-based InGaAs quantum dot solar cells with GaAs spacer layer fabricated using solid-source molecular beam epitaxy," Appl. Phys. Lett., vol.101, no.13, pp.133110-1–133110-4, Sept. 2012.
[27] S.M. Hubbard, C.D. Cress, C.G. Bailey, R.P. Raffaelle, S.G. Bailey, and D.M. Wilt, "Effect of strain compensation on quantum dot enhanced GaAs solar cells," Appl. Phys. Lett., vol.92, no.12, pp.123512-1–123512-3, March 2008.
[28] Y. Okada, T. Morioka, K. Yoshida, R. Oshima, Y. Shoji, T. Inoue, and T. Kita, "Increase in photocurrent by optical transitions via intermediate quantum states in direct-doped InAs/GaNAs strain-compensated quantum dot solar cell," J. Appl. Phys., vol.109, no.2, pp.024301-1–024301-5, Jan. 2011.
[29] A. Luque, A. Martí, and C. Stanley, "Understanding intermediate-band solar cells," Nature Photonics, vol.6, no.3, pp.146–152, March 2012.
[30] Y. Shoji, K. Narahara, H. Tanaka, T. Kita, K. Akimoto, and Y. Okada, "Effect of spacer layer thickness on multi-stacked InGaAs quantum dots grown on GaAs (311)B substrate for application to intermediate band solar cells," Appl. Phys. Lett., J. Appl. Phys., vol.111, no.7, pp.074305-1–074305-4, April 2012.
[31] T. Sugaya, T. Amano, M. Mori, and S. Niki, "Miniband formation in InGaAs quantum dot superlattice," Appl. Phys. Lett., vol.97, no.4, pp.043112-1–043112-3, July 2010.
[32] T. Sugaya, R. Oshima, K. Matsubara, and S. Niki, "InGaAs quantum dot superlattice with vertically coupled states in InGaP matrix," J. Appl. Phys., vol.114, no.1, pp.014303-1–014303-5, July 2013.
[33] T. Sugaya, O. Numakami, S. Furue, H. Komaki, T. Amano, K. Matsubara, Y. Okano, and S. Niki, "Tunnel current through a miniband in InGaAs quantum dot superlattice solar cells," Solar Energy Materials & Solar Cells, vol.95, no.10, pp.2920–2923, Oct. 2011.
[34] D. Gammon and D.G. Steel, "Optical studies of single quantum dots," Phys. Today, vol.55, no.10, pp.36–41, 2002.
[35] J.M. García, G. Medeiros-Ribeiro, K. Schmidt, T. Ngo, J.L. Feng, A. Lorke, J. Kotthaus, and P.M. Petroff, "Intermixing and shape changes during the formation of InAs self-assembled quantum dots," Appl. Phys. Lett., vol.71, no.14, p.2014, 1997.
[36] A. Zrenner, E. Beham, S. Stufler, F. Findeis, M. Bichler, and G. Abstreiter, "Coherent properties of a two-level system based on a quantum-dot photodiode," Nature, vol.418, no.6898, pp.612–614, 2002.
[37] D. Bimberg, M. Grundmann, and N.N. Ledentsov, Quantum Dot Heterostructures, Wiley, New York, 1998, ISBN: 978-0-471-97388-1.
[38] A. Barenco, C.H. Bennett, and P. Shor, "Elementary gates for quantum computation," Phys. Rev. A, vol.52, Issues 5, pp.3457–3467, 1995.
[39] H. Kamada, H. Gotoh, J. Temmyo, T. Takagahara, and H. Ando, "Exciton Rabi oscillation in a single quantum dot," Phys. Rev. Lett., vol.87, no.24, 2464, 2001.
[40] J.M. Villas-Bôas, S.E. Ulloa, and A.O. Govorov, "Decoherence of Rabi oscillations in a single quantum dot," Phys. Rev. Lett., vol.94, no.5, 057404, 2005.
[41] G. Chen, N.H. Bonadeo, D.G. Steel, D. Gammon, D.S. Katzer, D. Park, L.J. Sham, "Optically induced entanglement of excitons in a single quantum dot," Science, vol.289, Issues 5486, pp.1906–1909, 2000.
[42] G. Chen, T.H. Stievater, E.T. Batteh, X. Li, D.G. Steel, D. Gammon, D.S. Katzer, D. Park, and L.J. Sham, "Biexciton quantum coherence in a single quantum dot," Phys. Rev. Lett., vol.88, no.11, 117901, 2002.
[43] X. Li, Y. Wu, D. Steel, D. Gammon, T.H. Stievater, D.S. Katzer, D. Park, C. Piermarocchi, and L.J. Sham, "An all-optical quantum gate in a semiconductor quantum dot," Science, vol.301, Issues 5634, pp.809–811, 2003.
[44] K. Goshima, S. Yamauchi, K. Komori, I. Morohashi, and T. Sugaya, "Observation of exciton molecule consisting of two different excitons in coupled quantum dots," Appl. Phys. Lett., vol.87, no.25, p.253110, 2005.
[45] S. Yamauchi, K. Komori, I. Morohashi, K. Goshima, T. Sugaya, and T. Takagahara, "Observation of interdot correlation in single pair of electromagnetically coupled quantum dots," Appl. Phys. Lett., vol.87, no.18, p.182103, 2005.
[46] K. Goshima, K. Komori, T. Sugaya, and T. Takagahara, "Formation and control of a correlated exciton two-qubit system in a coupled quantum dot," Phys. Rev. B., vol.79, no.20, 205313, 2009.
[47] K. Goshima, S. Yamauchi, K. Komori, I. Morohashi, A. Shikanai, and T. Sugaya, "Exiciton Rabi oscillation in single pair of InAs/GaAs coupled quantum dots," Jpn. J. Appl. Phys., vol.46, no.4B, pp.2626–2628, 2007.

Kazuhiro Komori received the B.S., M.S., and Ph.D. degree in physical electronics from the Tokyo Institute of Technology, Tokyo, Japan, in 1984, 1986, 1989, respectively. During his Ph.D. work, he studied dynamic single mode (DSM) lasers and developed GaInAsP/InP distributed reflector (DR) lasers. In 1989, he joined the department of physical electronics, Tokyo Institute of Technology, as a Research Associate and engaged in the research on GaInAsP/InP dynamic single mode lasers and semiconductor laser amplifier. In 1994, he joined the Electrotechnical Laboratory (ETL), Tsukuba, Japan as a Senior Researcher. In 2001, he joined the National Institute of Advanced Industrial Science and Technology (AIST) as a group leader, and in 2010 as a deputy director in the Electronics and Photonics Research, Institute (ESPRIT) of AIST. He has been engaged in the study of optoelectronic devices and systems for the next-generation optical interconnects and optical communications. From 2013 to 2015, he temporally jointed in the Ministry of Economy, Trade and Industry (METI) as a director of Industry-University collaboration office. In 2015, he joined in the department of electronics and manufacturing of AIST as a senior planning manager. Dr. Komori is a member of the Institute of Electronics, Information, and Communication Engineers (IEICE) of Japan and Japan Society of Applied Physics. He received an Excellent Paper Award in 1988 from the Institute of Electronics, Information and Communication (IEICE) of Japan.

Takeyoshi Sugaya received the B.E., M.E. and Ph.D. degrees from Tsukuba University, Tsukuba, Japan, in 1989, 1991 and 1994, respectively. In 1994, he joined the Electrotechnical Laboratory, and was been working on MBE growth and quantum devices of compound semiconductors. He was a visiting researcher at the Arizona State University during 2000 – 2001 working on electron transport in quantum nanostructures. Currently, he is conducting research on the fabrication of quantum nano-structures and their application to next generation solar cell devices at Research Center for Photovoltaics, National Institute of Advance Industrial Science and Technology (AIST). Dr. Sugaya is a Member of the Japan Society of Applied Physics and the Institute of electronics, Information and Communication Engineers (IEICE).

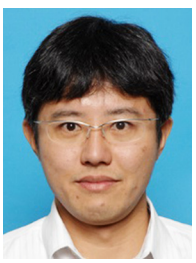

Takeru Amano was born in Tokyo, Japan, on July 26, 1976. He received the B.E., M.E. and Ph.D. degrees from Tokyo Institute of Technology, Tokyo, Japan, in 1999, 2001 and 2004, respectively. During his Ph.D. work, he studied micro-electro-mechanical systems (MEMS) optical filter and MEMS vertical-cavity surface-emitting lasers (VCSELs). In 2004, he joined the Ultrafast Optoelectronic Device Group, Photonics Research Center, National Institute of Advance Industrial Science and Technology (AIST) as a research member. Currently, he is conducting research on Quantum Dot fabrication, Quantum Dot fabrication and Quantum Dot Device. Dr. Amano received the IEEE LEOS Student Paper Award in 2000 and the IEEE EDS Student Paper Award in 2002. He is a Member of the Japan Society of Applied Physics and IEEE Photonics Society.

Keishiro Goshima received the B.S and M.S. electrical and electronics engineering, Aichi Institute of Technology (AIT), Japan, in 1998, 2000 and 2007, respectively. He joined postdoctoral studies from the Ultrafast Optoelectronic Device Group, Photonics Research Center, National Institute of Advance Industrial Science and Technology (AIST), Japan, during 2003-2010. He joined the Department of Reliability-based Information System engineering, Kagawa University, Japan, during 2010-2012. From 2012, he joined the Electrical and Electronics Engineering, Aichi Institute of Technology, Japan, as an assistant professor. His current research interests include optical devices using quantum dots.